Original Article

Quantification and Reduction of Respiratory Induced Artifact in Attenuation Correction of PET Data Using Respiration Averaged CT: a Simulation and Phantom Study

Fatemeh Sadat Fatemi Nasrollahi[1,2], Pardis Ghafarian[3,4], Parham Geramifar[5], Mohammad Reza Ay[1,2,*]

1- Department of Medical Physics and Biomedical Engineering, Tehran University of Medical Sciences, Tehran, Iran.

2- Research Center for Molecular and Cellular Imaging, Tehran University of Medical Sciences, Tehran, Iran.

3- Chronic Respiratory Diseases Research Center, National Research Institute of Tuberculosis and Lung Diseases (NRITLD), Shahid Beheshti University of Medical Sciences, Tehran, Iran.

4- PET/CT and Cyclotron Center, Masih Daneshvari Hospital, Shahid Beheshti University of Medical Sciences, Tehran, Iran.

5- Research Center for Nuclear Medicine, Tehran University of Medical Sciences, Tehran, Iran.

A B S T R A C T

Purpose- Respiratory-induced artifacts are dominant in Positron Emission Tomography/Computed Tomography (PET/CT) images. We investigated the impact of using the ACT data (respiration-averaged CT) in attenuation correction process. We evaluated the improvement in parameters such as maximum Standardized Uptake Value (SUV_{max}) and size in different respiratory traces for multiple lesion sizes in various locations of the thorax and abdomen.

Procedures- In simulation, the attenuation in PET sinograms were corrected using the end inhalation CT (EICT), end exhalation CT (EECT), and average CT (ACT) respectively. It should be noted that stationary PET images (without the respiratory motion) were reconstructed, and evaluated as the stationary truth. For the phantom study, a moving phantom was built mimicking the respiratory movement. The attenuation in uncorrected PET data was corrected using the three CT images mentioned above.

Results- In simulation, using EICT for attenuation correction, the respiration pattern with 35 millimeter diaphragm motion results in a %53 error in estimation in comparison with the stationary truth for a 9 millimeter lesion in the liver. The use of ACT in attenuation correction can reduce such amount of error in estimation up to %10 for this lesion. For the phantom study, using ACT for attenuation correction results in a significant improvement in Signal to Noise Ratio (SNR) and contrast (p-value<0.05). Besides, better was acquired for all the lesions.

Conclusion- The amount of respiratory induced errors in the quantified values of both and the volume of the tumor depends on the location of the tumor, its diameter, the amplitude of the diaphragm motion, and the CT image we use for attenuation correction. Overall, ACT shows better results in comparison with the aforementioned techniques for attenuation correction of PET data in thorax region.

1. Introduction

^{18}F-FDG PET/CT scanners are being widely used in the diagnosis and evaluation of neurologic disorders [1, 2], treatment response monitoring [3, 4], and treatment planning [5, 6]. This scanner has become a standard equipment, and a highly sensitive method providing comprehensive and reliable information on anatomical and functional properties of the patient's

Corresponding Author:
Mohammad Reza Ay, PhD
Department of Medical Physics and Biomedical Engineering, School of Medicine, Tehran University of Medical Sciences, Tehran, Iran.
Tel/Fax: (+98)2166907518
Email: Mohammadreza_ay@tums.ac.ir

body, which helps establishing more accurate diagnoses [7-9].

In PET/CT scanners, aside from the fact that the CT image is used to provide anatomical information, it is now commonly being utilized for the attenuation correction (AC) of PET images. In the past, radionuclide transmission scans were performed for the attenuation correction of the emission data, but now, the use of CT images for AC has lots of advantages. The generation of noise-free attenuation map, faster scan time, and the ability to collect uncontaminated post-injection transmission data are some of the advantages of CT-based attenuation correction [10-12]. However, the fast data acquisition of CT, compared to PET, causes data inconsistencies because of the respiratory motion, which is the primary source of misalignment between PET and CT. It leads to a tumor mislocalization and overestimation of tumor volume. CTAC may also bias the tracer distribution, which results in quantification errors. One example is the maximum Standardized Uptake Value (SUV_{max}), which is influenced by this misalignment [13-15].

Several works have investigated the magnitude of the respiratory-induced errors in quantitative parameters of a PET image. Depending on the lesion size, the lesion volume overestimation varies between 24% to 93% [13, 14]. Another research shows that the respiratory-induced blurring may cause SUV to be underestimated by 21% to 45% depending on the lesion size [16]. A simulation study indicates that a 35 mm diaphragm motion causes a 24% error in SUV_{max}, an average displacement of 7.6 mm, and a volume overestimation of 129% for a 9 mm liver lesion. The authors also demonstrated that the ACT-based attenuation correction shows lower errors in comparison with EICT or EECT when used for attenuation correction [17].

PET/CT imaging method is both time-consuming and expensive, but several studies have reported the usefulness of simulations for the evaluation of the imaging parameters [18-20]. One of the most efficient ways to study PET images in a simulation platform is using the 4D XCAT phantom and reconstructing its output using Software for the Tomographic Image Reconstruction (STIR) [17]. First of all, it is possible for the user to define a particular activity map for the human body in 4D XCAT phantom. We are able to study quantitative parameters of PET images in different organs, and especially with heterogeneous physiological uptake. Secondly, the XCAT phantom can model a common patient respiratory trace which is a crucial feature for this work.

In this study, we firstly examined the magnitude of the respiratory-induced errors for different lesion sizes, different diaphragm motions, and different attenuation correction maps. Then, we compared the PET/EECT and PET/EICT images with PET/ACT images to probe the enhancement in quantitative parameters of PET images. Afterwards, we examined our suggested method in a clinical environment using a respiration-modelling phantom.

2. Materials and Methods

2.1. Simulation Data

2.1.1. 4D XCAT Phantom

4D XCAT phantom is a realistic human body model which represents the human anatomy and physiology [20, 21]. In this study, alongside the activity maps, attenuation maps at 511 keV were generated and used for the attenuation and attenuation correction modelling later in reconstruction process. Each breathing cycle was considered to take 5 seconds, as it is typically observed in real patients. For each respiratory cycle, ten attenuation maps and ten activity maps were produced as the output of XCAT phantom, thus each images correspond to 0.5 seconds within a respiratory cycle.

2.1.2. Tumor Activity

In order to achieve realistic results, it is essential to employ real FDG concentrations in different organs of human body. These values are mentioned in Table 1. Moreover, these values are calculated from the SUV measurements in the literatures [22, 23]. A tumor to background activity ratio of 8:1 was implemented in previous studies [17, 24-26]. Next to this ratio, we also simulated and quantified the lesions with 4:1 tumor to background activity ratio, helping us investigate the quantitative parameters of PET images in low-uptake tumors. These tumors were in the same locations as the previous ones.

Table 1. Radioactivity concentration of organs.

Activity Concentration (kBq/cc)	Simulated Organ
2	Background
10	Myocardium
7	Spleen
7.8	Liver
1.6	Lung
6.5	Stomach
62.4	Liver lesion (8:1)
12.8	Lung lesion (8:1)
31.2	Liver Lesion (4:1)
6.4	Lung Lesion(4:1)

2.1.3. Tumor Size and Location

Due to the poor spatial resolution in PET images, and blurring caused by the respiratory motion, small lesions in thorax and abdomen are often misdiagnosed. Physicians are often advised not to use PET images for lesions smaller than 10 mm in diameter [27, 28]. As it is important to evaluate the impact of respiratory motion and CTAC on the quantification of different-sized tumors, we simulated lesions with different diameters in multiple locations of thorax region. The tumors had 9, 15 and 21 mm diameters. They were simulated in the following regions as illustrated in Figure 1.

1. The dome of the liver,

2. Lower lobe of the right lung,

3. Middle lobe of the right lung,

4. Lower lobe of the left lung,
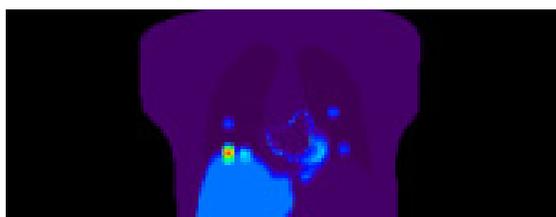
5. Middle lobe of the left lung.

Figure 1. The locations of the tumors in the radioactivity map. This show 15 mm lesions for 35 mm diaphragm motion.

2.1.4. Attenuation Correction of PET Images and Image Reconstruction

The attenuation correction and reconstruction of PET images were performed using STIR. The steps in this process are enumerated as follows: I. Generating sinograms out of the activity map using STIR ray tracing technique [29], II. Attenuating the sinogram using ACT III. Adding Poisson noise IV. Correcting the attenuation using EICT, EECT and ACT in three different images V. Reconstructing the PET image. For all tumor sizes and diaphragm motions, the stationary image (without the respiratory motion) was reconstructed as the reference image. The ordered subsets expectation maximization (OSEM) algorithm, as routinely engaged in commercial reconstruction softwares, was used for the reconstruction of the PET images involving 4 iterations and 20 subsets.

2.2. Phantom Study

2.2.1. PET/CT Scanner

PET/CT Biograph 6 (Siemens Healthcare) was used for our phantom study. The PET scanner has 39 detector rings made of LSO crystals. In total, it has 24336 crystals. The spatial resolution in PET scanner is 2 mm. The CT scanner has 6 detector rings with the spatial resolution of 1 mm. It covers 16.2 cm in axial and 70 cm in trans axial plane, and the time window in this system is set to be 4.5 ns.

2.2.2. Phantom Specifications

A specific phantom was designed and built to study the respiratory motion. It is made of methyl methacrylate (with the trade name of Plexiglass), and it has 4 main parts as listed below:

1. A cylinder with the height of 30 and the diameter of 20 cm. This cylinder was used to model the liver, and filled with radioactive water.

2. Another cylinder with the same height and diameter to model the right lung. It was filled with water and polystyrene to simulate the lung attenuation.

3. A circular plane which consists of 8 little cylinders with the height of 4.5 cm and diameter of 9, 11, 16 and 21 mm. In each diameter, there are 2 cylinders on this plane. These are used to simulate the lesions in diaphragm region.

4. Air compressor and electronic circuits to model the oscillatory respiration pattern.

Figure 2. The phantom which was built to study the respiratory motion. As it is seen the phantom is connected to a system which mimics the respiratory pattern as an oscillatory motion. The amplitude of the motion is 4.5 cm in 4.5 seconds as it is in real respiration.

The injected activity for standard patients ($\approx$70 kg) in our clinic is 370 MBq of FDG, resulting in a background activity concentration of 5.3 kBq/ml. The activity concentrations in the little cylindrical inserts were chosen in order to have a tumor to background ratio of 8:1 and 2:1. The data acquisition was performed in 3-dimentional (3D) for 3 minutes per bed position.

2.2.3. Image Reconstruction

Three CT images were acquired for the attenuation correction. The attenuation in uncorrected PET data was corrected using EICT, EECT and ACT. The properties of these 3 images are mentioned in Table 2. The images were reconstructed using OSEM + resolution recovery algorithm, involving 2 iterations and 21 subsets, with the Gaussian filter of 5 mm FWHM. All images were reconstructed into a 168×168 matrix with a 4 mm pixel size.

Table 2. The properties of different attenuation correction maps.

CT Type	kV	mAs	CTDIvol	DLP	Pitch
EICT	80	48	1.45	28	1
EECT	80	50	1.51	29	1
ACT	80	53	1.62	29	0.4

2.3. Data Analysis

2.3.1. Maximum Standardized Uptake Value

SUV_{max} is being widely used in clinical practice. This parameter shows the maximum uptake value in a volume of interest, which is often the tumor. It is defined in what follows:

$$SUV = \frac{\text{FDG activity concentration } (\frac{MBq}{ml})}{\text{Injected dose(MBq)/Phantom weight (g)}} \quad (1)$$

2.3.2. Tumor Size

Tumor size was calculated in AMIDE using the threshold of 20% maximum voxel intensity for the statistical calculations. This threshold achieves the optimal correlation of volume ratio, tumor length, and conformity index in 4D PET/CT images [30].

2.3.3. Contrast

When it comes to diagnosis, one of the essential image quality parameters is contrast. Contrast is calculated using equation 2 [31].

$$Contrast = \frac{C_{VOI}}{C_{Background}} \quad (2)$$

Where C_{VOI} refers to maximum activity concentration within a lesion VOI, and $C_{Background}$ is the mean activity in background ROIs.

2.3.4. Signal to Noise Ratio

Signal to Noise Ratio (SNR) is also considered to be important in clinical practice and accurate diagnosis. It is calculated according to equation 3 [31].

$$SNR = \frac{C_{VOI} - C_{Background}}{SD_{Background}} \quad (3)$$

Where C_{VOI} refers to maximum activity concentration within a lesion VOI, $C_{Background}$ is the mean activity in the background ROIs, and $SD_{Background}$ is the standard deviation of activity in the background ROIs.

3. Results

3.1. Simulation

The tumors in thorax region are moved due to the respiratory motion. Since the PET data is acquired over a couple of respiratory cycles, lesions are expected to be blurred, and hence their volume is miscalculated. As described in the previous section, in our analysis, tumor volume was calculated in AMIDE software with the threshold of 20% maximum voxel intensity. Figure 3 shows the difference between the tumor volume in PET/ACT and PET/STCT.
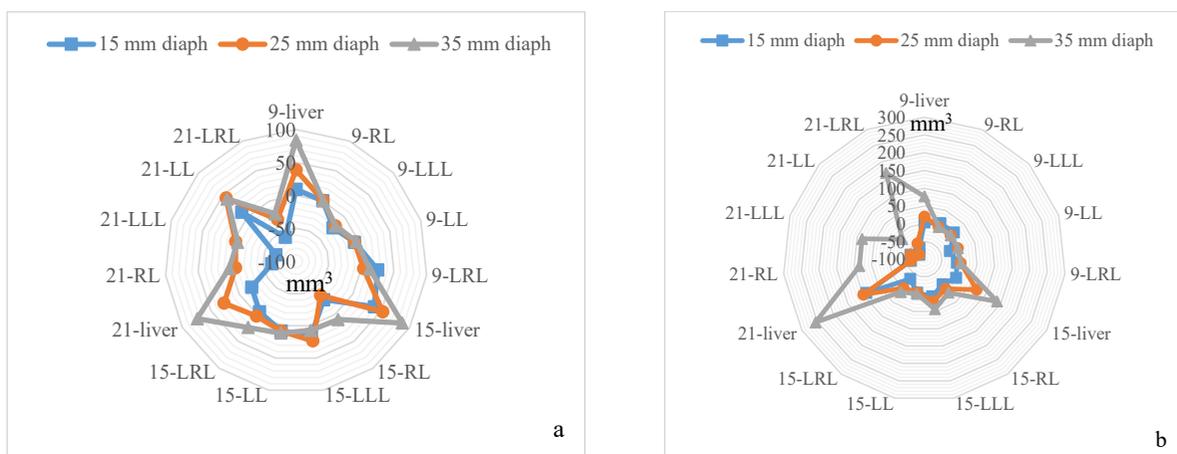

Figure 3. the difference between the volume of lesions in PET/ACT and PET/STCT in 15 lesions for 8:1 lesion to background ratio (a) and 4:1 lesion to background ratio (b). RL shows right lung, LLL shows the lower lobe of the left lung, LL shows the left lung, and LRL shows the lower lobe of the right lung.

Figure 3 shows that as we increase the amplitude of diaphragm motion, the difference in the tumor volume between PET/ACT and PET/STCT increases. Both plots also indicate that the difference in volume between PET/ACT and PET/STCT is maximum in liver lesions. The lesions in the lower lobe of both lungs have had the maximum difference in second place. Therefore, it is observed that lesions in diaphragm region are most influenced by the respiratory motion.

Figure 4 shows the percent error in SUV_{max} in PET/EICT, PET/EECT, and PET/ACT relative to stationary image as the ground truth. As it is demonstrated in this figure, with the increase of the amplitude of the diaphragm motion, the highest error elevates from 23% to 53%. In all three diaphragm motions, it is seen that the PET/EICT has the highest error in estimating SUV_{max}. Besides, PET/ACT shows lower errors in comparison with PET/EICT. Obviously, the error is strongly dependent on the tumor size, location, and the choice of attenuation map. For example, PET/EECT shows slightly lower errors in some tumors in comparison with PET/ACT, but it is not statistically significant (p-value=0.061, 0.087, 0.156 for lesion sizes of 9, 15 and 21 mm respectively). Nonetheless, the use of ACT instead of EICT appears to be significantly useful in reduction of respiratory-induced errors in estimating SUV_{max} (p-value=0.001, 0.008, 0.023 for lesion sizes of 9, 15 and 21 mm respectively).
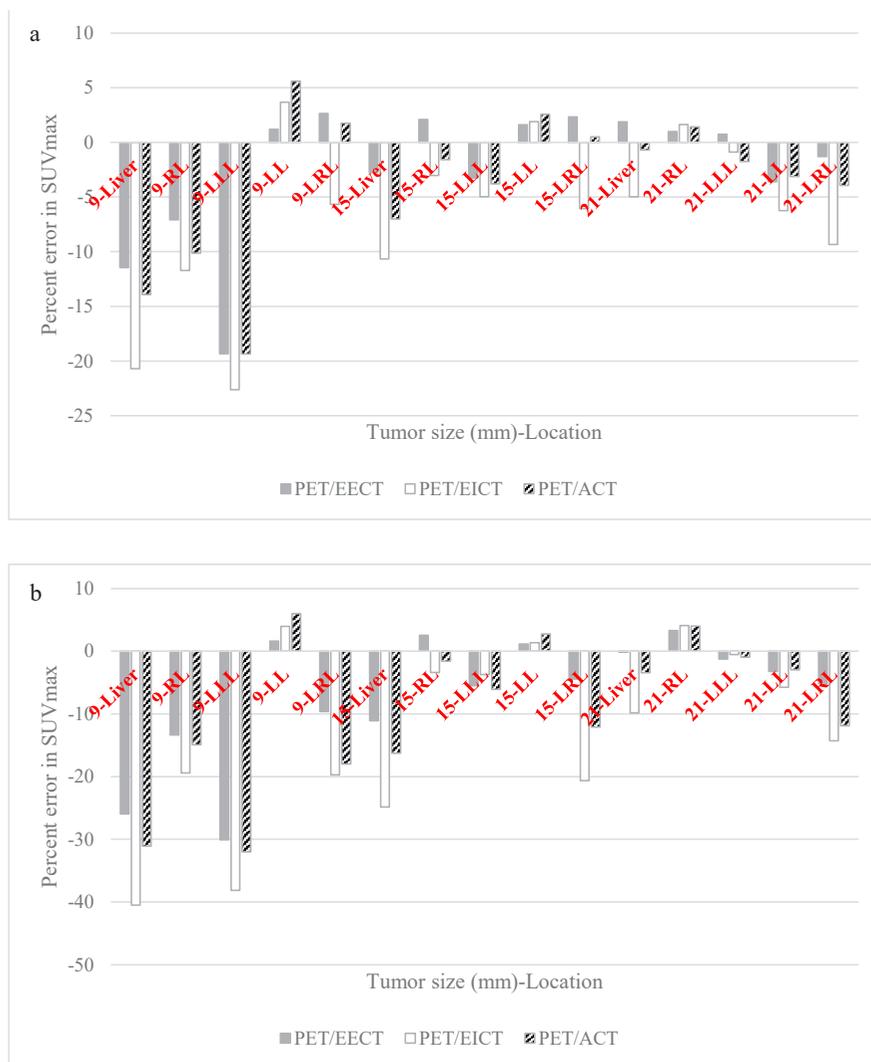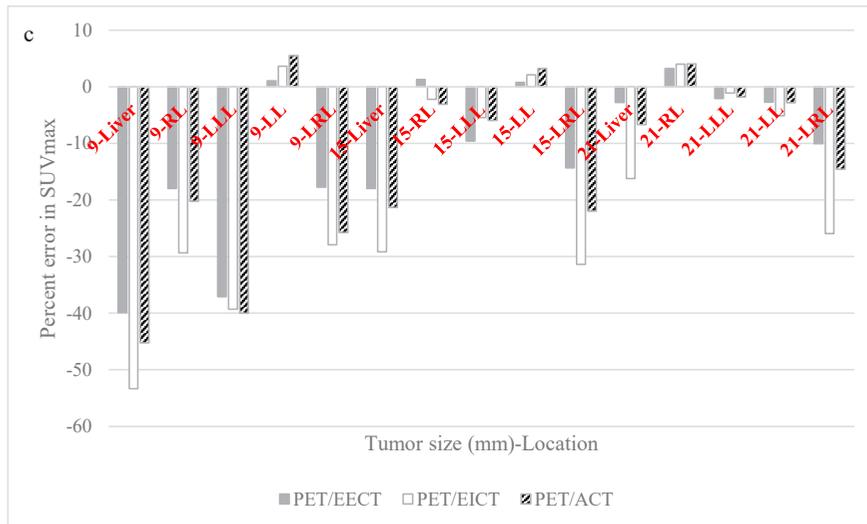
Figure 4. Percent error in SUV$_{max}$ in PET/EICT, PET/EECT, and PET/ACT relative to the stationary truth for 15 mm diaphragm motion (a), 25 mm diaphragm motion (b), and 35 mm diaphragm motion (c).

3.2. Phantom Study

The attenuation in uncorrected PET data was corrected using 3 different CT images, as it is seen in Figure 5. It is visually evident that the lesion sizes are minimized in PET/EICT. A hot area around the lesions is also observable in this image, which is because of the outer edge of our phantom. This causes the attenuation coefficients to be overestimated, and later in attenuation correction process, the uptake in these regions are overestimated too. This influences the SUV in lesions as well. To find a way to solve this issue, we compared the uptake in uniform regions with this region with overestimated ACFs, and calculated the correction factor. This factor was multiplied by all the results in these slices.
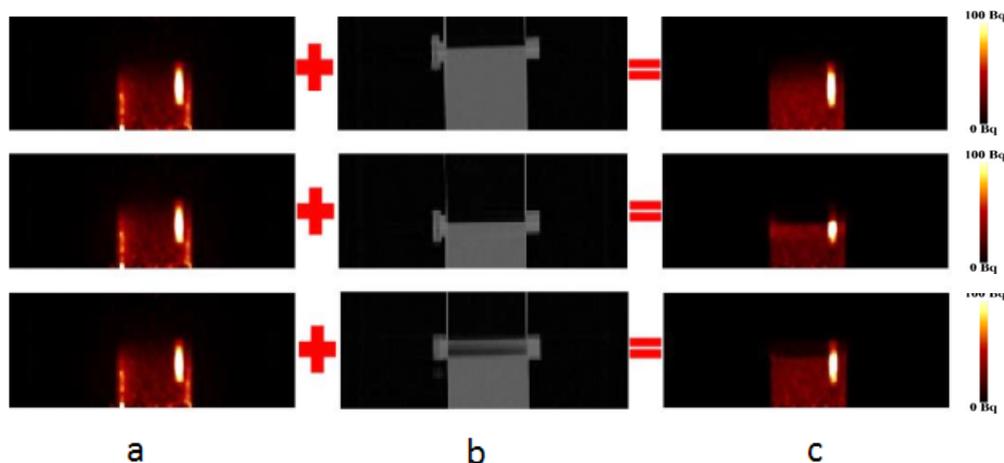
Figure 5. The uncorrected PET in column (a), EECT, EICT and ACT in column (b), and corrected PET images in column (c).

Figure 6 shows the SUV$_{max}$ for different sizes and lesions to background ratios. As it is shown, SUV in PET/ACT is higher than the other two images, which is statistically significant (p-value=0.012). While comparing PET/EECT with PET/EICT, we perceive that PET/EECT gives a higher SUV, which is consistent with the simulation results.
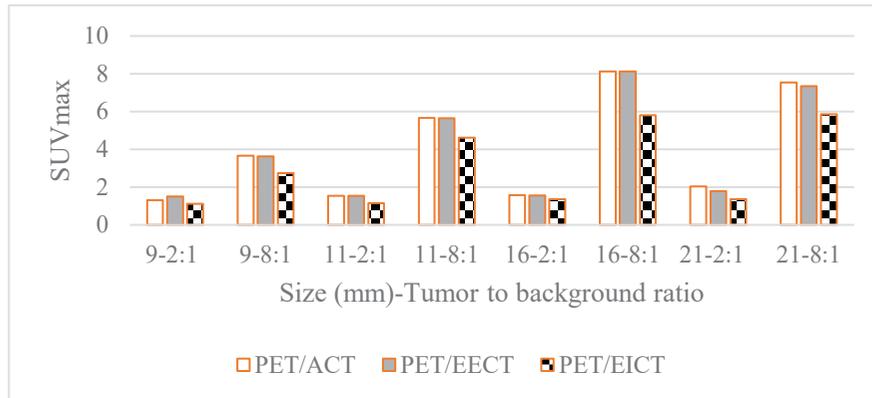
Figure 6. SUV$_{max}$ for 9, 11, 16, and 21 mm lesions in phantom study.

Figure 7 shows the contrast and signal to noise ratio in all 8 lesions. PET/ACT shows a better contrast and SNR in all the lesions. From a statistical point of view, the use of ACT instead of EECT and EICT for attenuation correction of PET images has improved contrast and SNR significantly (p-value= 0.025, 0.012 for PET/EECT and PET/EICT respectively).
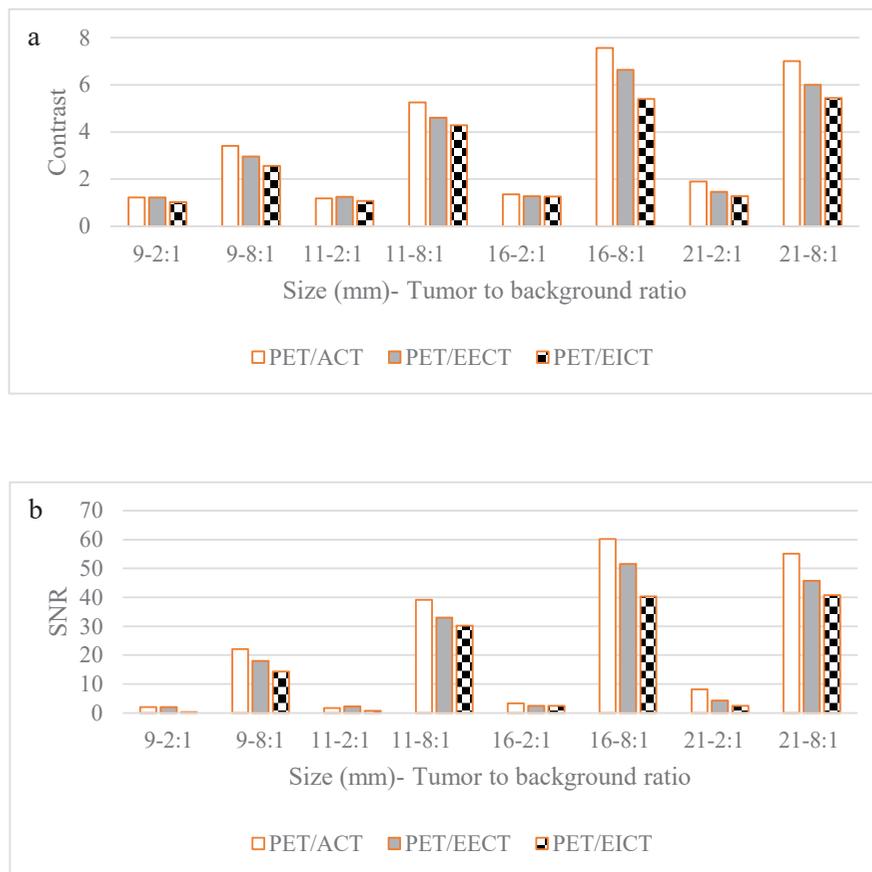

Figure 7. Contrast (a) and SNR (b) in PET/ACT, PET/EECT, and PET/EICT for all 8 lesions.

4. Discussion

A major pitfall in PET/CT imaging is the mismatch between PET and CT data due to the respiratory motion as well as the patient's bulk motion. As such, misaligned CT can project a part of the diaphragm onto the thorax region, leading to clinical misinterpretation of the corrected PET data. One approach to reduce the effect of misalignment due to the different temporal resolution between activity and attenuation maps, is to use the average CT over a respiratory cycle for the attenuation correction. Also, the previous studies have shown the benefits of using ACT-based attenuation correction of PET data in reducing the respiratory-induced errors [17, 32, 33].

PET data is acquired over a couple of respiratory cycles; thereupon the lesion volume change is one of the consequences of respiratory motion. A CT image, on the other hand, is acquired in a single phase of the respiratory cycle, hence the CTAC process causes errors and artifacts. In the simulation part, as it was shown in Figure 3, when the amplitude of the diaphragm motion increases, the estimated tumor volume increases. The average change in tumor volume varies between 30 mm^3 to 61 mm^3 for 4:1 lesion to background ratio, and between 25 mm^3 to 27 mm^3 for 8:1 lesion to background ratio, which shows how much low uptake tumors are sensitive to motion. This happens due to the organ movement caused by respiration and blurring in thorax region. Also, this volume change is maximized in the liver and the lower lobe of both lungs, because in these places the amplitude of the respiratory motion is maximized. It varies between 77 mm^3 to 86 mm^3 for liver lesions, and between 2 mm^3 to 23 mm^3 for lesions in the lower lobe of both lungs.

Figure 4.a, 4.b and 4.c illustrate that in simulated data, the PET/ACT has lower SUV_{max} errors in comparison with PET/EICT and PET/EECT. We investigated that 9 mm tumors have higher errors in estimating SUV. This indicates that smaller tumors are more sensitive to respiratory motion, and in order to be able to diagnose them, it is necessary to optimize the attenuation correction process using ACT based attenuation correction. It is seen that ACT significantly reduces the error in estimating SUV_{max} (p-value<0.05 for all 3 tumor diameters), which suggests that ACT-based attenuation correction can be useful, especially in tumors that are located in diaphragm region.

In our phantom study we observed that PET/ACT has higher SUVs. This is because the temporal resolution of the uncorrected PET data and ACT is the same, so the attenuation correction coefficients are estimated more accurately, hence SUV is calculated to be higher in PET/ACT. Regarding image quality parameters, Figure 7.a and 7.b show that PET/ACT has better contrast and SNR relative to the other two images. In comparison with PET/EECT, SNR and contrast improved in PET/ACT by 22% and 11% respectively (p-value<0.05). Furthermore, in comparison with PET/EICT, SNR and contrast improved in PET/ACT by 42% and 26% respectively (p-value<0.05).

5. Conclusion

In this study, we examined elaborate measurements and analysis of SUV_{max} and volume for multiple lesions for a common patient respiratory5 trace with respect to PET/STCT (stationary truth) as a surrogate for the true values. Different lesion sizes, lesion locations, and diaphragm motions were simulated, and different choices of attenuation maps were characterized and analyzed in simulated attenuation corrected PET images. In our phantom study, different lesion sizes and lesion to background ratios were considered as well. Both the simulation results and phantom study indicate that respiratory motion can significantly decrease the accuracy of PET/CT quantitative imaging, which has adverse effects on diagnosis, radiation treatment planning, and treatment response monitoring [30, 34]. They also demonstrate that ACT is useful for the attenuation correction of PET images in diaphragm region. Regarding temporal resolution, ACT is the most accurate, and gives lower errors in estimating tumor quantification parameters.

Acknowledgements

References

1- W. Chen, "Clinical applications of PET in brain tumors," *Journal of nuclear medicine,* vol. 48, pp.

1468-1481, 2007.

2- Y. Tai and P. Piccini, "Applications of positron emission tomography (PET) in neurology," *Journal of Neurology, Neurosurgery & Psychiatry,* vol. 75, pp. 669-676, 2004.

3- T. Okuma, T. Matsuoka, T. Okamura, Y. Wada, A. Yamamoto, Y. Oyama*, et al.*, "18F-FDG small-animal PET for monitoring the therapeutic effect of CT-guided radiofrequency ablation on implanted VX2 lung tumors in rabbits," *Journal of Nuclear Medicine,* vol. 47, pp. 1351-1358, 2006.

4- L. K. Shankar, J. M. Hoffman, S. Bacharach, M. M. Graham, J. Karp, A. A. Lammertsma*, et al.*, "Consensus recommendations for the use of 18F-FDG PET as an indicator of therapeutic response in patients in National Cancer Institute Trials," *Journal of Nuclear Medicine,* vol. 47, pp. 1059-1066, 2006.

5- E. C. Ford, J. Herman, E. Yorke, and R. L. Wahl, "18F-FDG PET/CT for image-guided and intensity-modulated radiotherapy," *Journal of Nuclear Medicine,* vol. 50, pp. 1655-1665, 2009.

6- M. MacManus, U. Nestle, K. E. Rosenzweig, I. Carrio, C. Messa, O. Belohlavek*, et al.*, "Use of PET and PET/CT for radiation therapy planning: IAEA expert report 2006–2007," *Radiotherapy and oncology,* vol. 91, pp. 85-94, 2009.

7- B. M. Fischer, J. Mortensen, and L. Højgaard, "Positron emission tomography in the diagnosis and staging of lung cancer: a systematic, quantitative review," *The lancet oncology,* vol. 2, pp. 659-666, 2001.

8- D. Groheux, S. Giacchetti, M. Delord, E. Hindié, L. Vercellino, C. Cuvier*, et al.*, "18F-FDG PET/CT in staging patients with locally advanced or inflammatory breast cancer: comparison to conventional staging," *Journal of Nuclear Medicine,* vol. 54, pp. 5-11, 2013.

9- E. M. Rohren, T. G. Turkington, and R. E. Coleman, "Clinical applications of PET in oncology," *Radiology,* vol. 231, pp. 305-332, 2004.

10- M. Abella, A. M. Alessio, D. A. Mankoff, L. R. MacDonald, J. J. Vaquero, M. Desco*, et al.*, "Accuracy of CT-based attenuation correction in PET/CT bone imaging," *Physics in medicine and biology,* vol. 57, p. 2477, 2012.

11- P. Kinahan, D. Townsend, T. Beyer, and D. Sashin, "Attenuation correction for a combined 3D PET/CT scanner," *Medical physics,* vol. 25, pp. 2046-2053, 1998.

12- P. E. Kinahan, B. H. Hasegawa, and T. Beyer, "X-ray-based attenuation correction for positron emission tomography/computed tomography scanners," in *Seminars in nuclear medicine*, 2003, pp. 166-179.

13- Y. E. Erdi, S. A. Nehmeh, T. Pan, A. Pevsner, K. E. Rosenzweig, G. Mageras*, et al.*, "The CT motion quantitation of lung lesions and its impact on PET-measured SUVs," *Journal of Nuclear Medicine,* vol. 45, pp. 1287-1292, 2004.

14- S. A. Nehmeh and Y. E. Erdi, "Respiratory motion in positron emission tomography/computed tomography: a review," in *Seminars in nuclear medicine*, 2008, pp. 167-176.

15- B. Thorndyke, E. Schreibmann, A. Koong, and L. Xing, "Reducing respiratory motion artifacts in positron emission tomography through retrospective stacking," *Medical physics,* vol. 33, pp. 2632-2641, 2006.

16- L. Boucher, S. Rodrigue, R. Lecomte, and F. Bénard, "Respiratory gating for 3-dimensional PET of the thorax: feasibility and initial results," *Journal of Nuclear Medicine,* vol. 45, pp. 214-219, 2004.

17- P. Geramifar, M. S. Zafarghandi, P. Ghafarian, A. Rahmim, and M. R. Ay, "Respiratory-induced errors in tumor quantification and delineation in CT attenuation-corrected PET images: effects of tumor size, tumor location, and respiratory trace: a simulation study using the 4D XCAT phantom," *Molecular Imaging and Biology,* vol. 15, pp. 655-665, 2013.

18- P. Geramifar, M. Ay, M. S. Zafarghandi, S. Sarkar, G. Loudos, and A. Rahmim, "Investigation of time-of-flight benefits in an LYSO-based PET/CT scanner: A Monte Carlo study using GATE," *Nuclear Instruments and Methods in Physics Research Section A: Accelerators, Spectrometers, Detectors and Associated Equipment,* vol. 641, pp. 121-127, 2011.

19- P. Geramifar, M. R. Ay, M. Shamsaie Zafarghandi, G. Loudos, and A. Rahmim, "Performance comparison of four commercial GE discovery PET/CT scanners: A monte carlo study using GATE," *Iranian Journal of Nuclear Medicine,* vol. 17, pp. 26-33, 2009.

20- W. Segars, G. Sturgeon, S. Mendonca, J. Grimes, and B. M. Tsui, "4D XCAT phantom for multimodality imaging research," *Medical physics,* vol. 37, pp. 4902-4915, 2010.

21- W. P. Segars, M. Mahesh, T. J. Beck, E. C. Frey, and B. M. Tsui, "Realistic CT simulation using the 4D XCAT phantom," *Medical physics,* vol. 35, pp. 3800-3808, 2008.

22- C. D. Ramos, Y. E. Erdi, M. Gonen, E. Riedel, H. W. Yeung, H. A. Macapinlac*, et al.*, "FDG-PET

standardized uptake values in normal anatomical structures using iterative reconstruction segmented attenuation correction and filtered back-projection," *European Journal of Nuclear Medicine and Molecular Imaging,* vol. 28, pp. 155-164, 2001.

23- S. Zincirkeser, E. Şahin, M. Halac, and S. Sager, "Standardized uptake values of normal organs on 18F-fluorodeoxyglucose positron emission tomography and computed tomography imaging," *Journal of international medical research,* vol. 35, pp. 231-236, 2007.

24- S. Nehmeh, H. El-Zeftawy, C. Greco, J. Schwartz, Y. Erdi, A. Kirov, *et al.*, "An iterative technique to segment PET lesions using a Monte Carlo based mathematical model," *Medical physics,* vol. 36, pp. 4803-4809, 2009.

25- C. Liu, L. A. Pierce II, A. M. Alessio, and P. E. Kinahan, "The impact of respiratory motion on tumor quantification and delineation in static PET/CT imaging," *Physics in medicine and biology,* vol. 54, p. 7345, 2009.

26- F. Lamare, T. Cresson, J. Savean, C. C. Le Rest, A. Reader, and D. Visvikis, "Respiratory motion correction for PET oncology applications using affine transformation of list mode data," *Physics in medicine and biology,* vol. 52, p. 121, 2006.

27- M. P. Rivera, F. Detterbeck, and A. C. Mehta, "Diagnosis of lung cancer: the guidelines," *CHEST Journal,* vol. 123, pp. 129S-136S, 2003.

28- W. M. Alberts, "Diagnosis and management of lung cancer executive summary: ACCP evidence-based clinical practice guidelines," *CHEST Journal,* vol. 132, pp. 1S-19S, 2007.

29- R. Manber, K. Thielemans, B. F. Hutton, A. Barnes, S. Ourselin, S. Arridge, *et al.*, "Practical PET respiratory motion correction in clinical PET/MR," *Journal of Nuclear Medicine,* vol. 56, pp. 890-896, 2015.

30- Y.-C. Wang, T.-C. Hsieh, C.-Y. Yu, K.-Y. Yen, S.-W. Chen, S.-N. Yang, *et al.*, "The clinical application of 4D 18F-FDG PET/CT on gross tumor volume delineation for radiotherapy planning in esophageal squamous cell cancer," *Journal of radiation research,* vol. 53, pp. 594-600, 2012.

31- G. Akamatsu, K. Ishikawa, K. Mitsumoto, T. Taniguchi, N. Ohya, S. Baba, *et al.*, "Improvement in PET/CT image quality with a combination of point-spread function and time-of-flight in relation to reconstruction parameters," *Journal of Nuclear Medicine,* vol. 53, pp. 1716-1722, 2012.

32- A. M. Alessio, S. Kohlmyer, K. Branch, G. Chen, J. Caldwell, and P. Kinahan, "Cine CT for attenuation correction in cardiac PET/CT," *Journal of Nuclear Medicine,* vol. 48, pp. 794-801, 2007.

33- T. Pan, O. Mawlawi, S. A. Nehmeh, Y. E. Erdi, D. Luo, H. H. Liu, *et al.*, "Attenuation correction of PET images with respiration-averaged CT images in PET/CT," *Journal of Nuclear Medicine,* vol. 46, pp. 1481-1487, 2005.

34- D. Han, J. Yu, Y. Yu, G. Zhang, X. Zhong, J. Lu, *et al.*, "Comparison of 18 F-fluorothymidine and 18 F-fluorodeoxyglucose PET/CT in delineating gross tumor volume by optimal threshold in patients with squamous cell carcinoma of thoracic esophagus," *International Journal of Radiation Oncology* Biology* Physics,* vol. 76, pp. 1235-1241, 2010.